

Water-methanol mixture under confinement

Roger Bellido

*Facultat de Física, Universitat de Barcelona, Diagonal 645, 08028 Barcelona.**

Advisor: Giancarlo Franzese

(Dated: 06/07/2022)

Water pollution and renewable energy sources are a matter of broad concern, both environmental challenges for our society. For its applications in the chemical and pharmaceutical industry, production of synthetic fibers and plastic, and as a fuel additive, methanol attracts interest for how to model its properties when mixed with water. Here, we consider a minimalistic model for a water-methanol mixture confined between two parallel graphene nanosheets and analyze the diffusion coefficient of each component as the slit-pore's width δ increases. We find that layering in the hydrophobic pore induces segregation between the two components. The methanol apolar moiety accumulates near the pore walls, while water populates more in the central layer away from the hydrophobic walls. Furthermore, both liquids have a diffusion coefficient that changes non-monotonically with δ , with water always diffusing faster than methanol. Changes in the pore widths affect the two mixture components in different amounts, suggesting the possibility of an efficient method for methanol-water separation based on a physical procedure.

I. INTRODUCTION

Although given for granted in our everyday life, water is a limited resource under the threat of uncontrolled pollution and desertification for climate change. Hence, seeking new ways to provide methods to filter and obtain purified water is of the utmost importance. A recent promising method is to use graphene-based membranes, which affect the dynamics of the confined fluids compared to bulk [1].

More generally, the problem of separating different components of aqueous mixtures is relevant in many industrial processes and applications. Here, we focus on methanol/water mixtures. It is widely used in food processing, preservation, pharmaceutical, and chemical industries. In some processes, methanol is mixed with water and their separation is necessary for further use of both. For example, methanol is added to gasoline to reduce exhaust gases emission or is used in fuel cells to obtain electrical energy from chemical energy [2]. The separation of methanol from water is usually performed by inefficient and energetically-intensive distillation. Hence, recently several groups are investigating theoretically alternative separation methods, e.g., as in Refs. [2–4].

Water is an anomalous liquid because many of its properties are counterintuitive [5]. Apart from its thermodynamic anomalies, including the increasing response functions for decreasing temperatures approaching 0°C and in the supercooled liquid phase, water has dynamical

anomalies. In particular, under slit-pore confinement, its thermal diffusion constant D_{\parallel} parallel to the slits has a non-monotonic behavior when the slit-pore width δ changes below 1.5 nm [6]. Although the mechanism leading to the variation of D_{\parallel} in water is unique and different from other liquids, recent simulations show that this behavior can be observed, to some extent, also in simple liquids and other anomalous liquids [7]. In particular, the anomalous liquids have water-like properties, such as isothermal diffusion-constant maxima, as well as structural and thermodynamic anomalies and are represented as soft-core isotropic potentials [8]. For this reason, they are often used as a zero-approximation model for water. Here we will consider the continuous shouldered well (CSW) potential [9], already adopted for studies of water-methanol mixtures [10].

Methanol is the smallest alcohol, with an apolar methyl group (CH_3) and a polar hydroxyl group (OH). It is fully miscible with water for all compositions. It fully integrates into the water's hydrogen bond network because it forms hydrogen bonds of similar strength and length and is similar to water in size. Following Urbic and co-workers, we model it with two pseudoatoms (OH and CH_3) of the same size and in a fixed position [10–12]. The hydrogen-bond forming hydroxyl group interacts via a CSW potential, while the hydrophobic methyl group via a Lennard-Jones (LJ) potential, as described in the following.

The present work is organized as follows. First, we present the Molecular Dynamics (MD) methodology that allows us to fix the thermodynamical control parameters (e.g., temperature T , total volume V , and mixture composition) and calculate relevant observables, such as the

*Electronic address: rbellipe20@alumnes.ub.edu

diffusion constant. The reason behind the choosing of this simulation method is to be able to observe and comprehend the mesoscale properties of the system.

Then, we define the CSW water-like liquid and the Urbic methanol model. We set the confining slit-pore geometry and describe the interactions between the mixture and the graphene. After a preliminary calculation of the bulk diffusion coefficient, D , for the CSW model, we simulate the mixture under confinement, calculate the diffusion constant, D_{\parallel} , parallel to the graphene slit-pore for the nanoconfined components of the mixture, and discuss the results. Finally, we present our conclusions about the possibility of separating the two components via nanoconfinement and the perspectives of this work.

II. METHODOLOGY AND SIMULATIONS

A. Molecular Dynamics

Nowadays MD simulations are a standard tool to investigate the thermodynamics and dynamics of atomistic or coarse-grained models in many disciplines, such as, e.g., liquid-state theory, soft-matter, biophysics, and biochemistry. To this goal, several software suites are constantly developed by the international scientific community and are available for free. Here, we will use the MD tool LAMMPS (**L**arge-scale **A**tomic/**M**olecular **M**assively **P**arallel **S**imulator). It is a simulation code focused on material modeling, designed to run efficiently on parallel computers. It is open-source, freely distributed under the terms of the GNU Public License Version 2 (GPLv2) [13].

We perform our main simulations in the canonical ensemble where the total number N of the atoms of the two components, V and T are constant (NVT ensemble). We integrate in time the Newton equations of motion via the Leap-Frog algorithm and control the temperature via a Nosé-Hoover thermostat, discussed in Appendix A. We calculate the pressure as

$$P \equiv \frac{1}{3V} \left(\sum_i m_i v_i^2 + \sum_{i>j} \mathbf{r}_{ij} \mathbf{F}_{ij} \right), \quad (1)$$

where m_i and v_i are the mass and the velocity, respectively, of the particle i , \mathbf{r}_{ij} and \mathbf{F}_{ij} are the distance and the force, respectively, between the particles i and j .

In bulk, we use also the NPT ensemble, where V is free to change and we control P via a barostat. LAMMPS uses the inertia W to determine the relaxation rate of the barostat:

$$W \equiv (N + 1)k_B T_{\text{target}} P_{\text{damp}}^2 \quad (2)$$

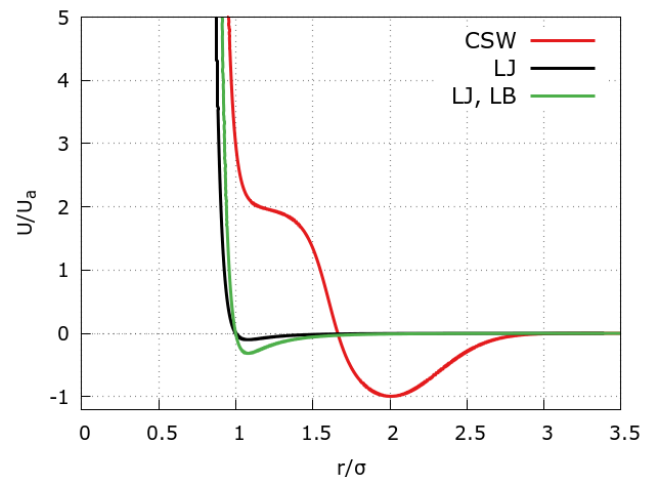


FIG. 1: Interactions potentials between the particles of the simulation. The continuous shouldered well (CSW) potential (red line) has two characteristic length-scales (the repulsive shoulder and the attractive well) that mimic the hydrogen-bond interaction and are responsible for the water-like properties. The CSW is used also for all the interactions involving the formation of a hydrogen bond with methanol and water. The Lennard-Jones (LJ, black line) and LJ with Lorentz-Berthelot (LB) mixing rules (green line) are the interaction potentials for the methyl-methyl and methyl-hydroxyl interactions, respectively.

where N is the number of particles, k_B the Boltzmann constant, T_{target} the target temperature of the barostat and P_{damp} the timescale over which the pressure equilibrates.

Because we adopt a diatomic model for the methanol, we need to update the molecular configurations imposing the constrain of constant distance for the position of the two methanol groups. To this goal, we use the SHAKE algorithm, which recursively imposes the constraint, as described in Appendix B and C. We performed the simulations on a dedicated cluster of GPUs of the *Laboratorio de Supercomputación en Física Estadística*, an infrastructure shared by the advisor with other researchers.

We set a simulation box with periodic boundary conditions centered at the origin of coordinates, with $-x_{\text{lim}} < x < x_{\text{lim}}$, $-y_{\text{lim}} < y < y_{\text{lim}}$ and $-z_{\text{lim}} < z < z_{\text{lim}}$. The extremes of the coordinates are free to change during the NPT simulations, while are fixed in the NVT calculations.

Generally, in our simulations, we will do a first run in order to thermalize the system, that is: from a first artificially created configuration, we let the system evolve into an equilibrated state. Once it is reached, a second run is done to obtain enough data to extract useful measurements.

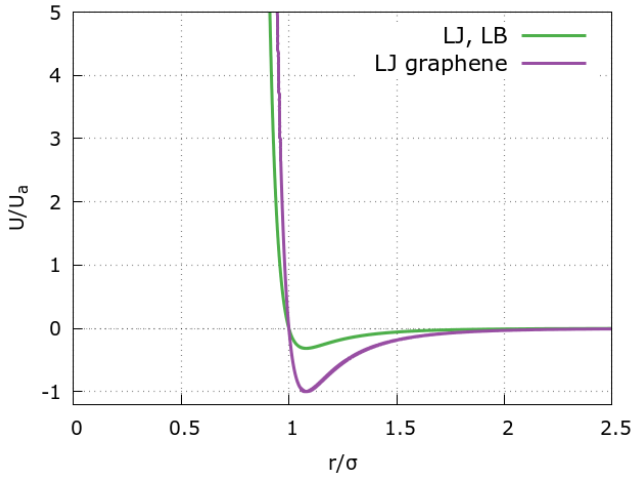


FIG. 2: The LJ interaction of graphene atoms and fluid particles (violet line) compared with the LJ, LB potential in Fig.1 (green line).

B. The coarse-grained models for the mixture

We adopt the CSW model for water-like liquids, represented in Fig. 1 (red line), where soft-spheres, with a hard-core of diameter a and a soft-shell with radius $2a$, interact via the core-softened potential [9],

$$U_{\text{CSW}}(r) \equiv k_1 + k_2 + k_3 \quad (3)$$

$$k_1 \equiv \frac{U_R}{1 + \exp\left(\frac{\Delta(r-R_R)}{a}\right)} \quad (4)$$

$$k_2 \equiv -U_A \exp\left(-\frac{(r-R_A)^2}{2\delta_A^2}\right) \quad (5)$$

$$k_3 \equiv U_A \left(\frac{a}{r}\right)^{24} \quad (6)$$

with parameters

$$\begin{aligned} \frac{U_R}{U_A} &= 2, \quad \frac{R_R}{a} = 1.6 \\ \frac{R_A}{a} &= 2, \quad \left(\frac{\delta_A}{a}\right)^2 = 0.1 \\ \Delta &= 15. \end{aligned}$$

For the methanol, we use the coarse-grained (dimer) model by Urbic and co-workers [10–12] with the two pseudoatoms (OH and CH₃) at a fixed distance (dumbbell model). The different groups have the following interactions:

- apolar-apolar (CH₃-CH₃): LJ potential, U_{LJ} ,
- CH₃-OH, CH₃-H₂O: LJ with Lorentz-Berthelot (LB) mixing rules,

- OH-OH, OH-H₂O, H₂O-H₂O: CSW potential,

where

$$U_{\text{LJ}}(r) \equiv \frac{4}{3} 2^{2/3} \epsilon \left[\left(\frac{\sigma}{r}\right)^{24} + \left(\frac{\sigma}{r}\right)^6 \right] \quad (7)$$

with

$$\begin{aligned} \frac{\sigma_{\text{LJ}}}{a} &= 1.0 \\ \frac{\epsilon_{\text{LJ}}}{U_A} &= 0.1, \end{aligned}$$

and the LB mixing rules

$$\begin{aligned} \sigma_{\text{mix}} &\equiv \frac{1}{2}(\sigma_{\text{LJ}} + a) \\ \epsilon_{\text{mix}} &\equiv \sqrt{\epsilon_{\text{LJ}} U_A}. \end{aligned}$$

In the following we adopt dimensionless units:

$$\begin{aligned} T^* &\equiv \frac{k_B T}{U_A}, \\ \rho^* &\equiv \rho a^3, \quad \text{where} \quad \rho \equiv \frac{N}{V}, \\ P^* &\equiv \frac{a^3}{U_A} P, \\ t^* &\equiv \left(\frac{a^2 m}{U_A}\right)^{\frac{1}{2}} \end{aligned}$$

C. The model for the graphene slit pore

Each of the two graphene sheets is modeled as a honeycomb lattice, as in the atomic structure of the material. The unit cell is defined by the vectors

$$\vec{a}_1 \equiv a\sqrt{3} \left(\frac{\sqrt{3}}{2}, \frac{1}{2}\right), \quad \vec{a}_2 \equiv a\sqrt{3} \left(\frac{\sqrt{3}}{2}, -\frac{1}{2}\right). \quad (8)$$

The atoms are positioned via linear combinations of the unit cell vectors ($\alpha_i \vec{a}_1 + \beta_j \vec{a}_2$) with $i, j = 1, 2$ and

$$\alpha_1 = 0, \beta_1 = 0; \alpha_2 = \frac{1}{3}, \beta_2 = \frac{1}{3}. \quad (9)$$

Each graphene atom interacts with the fluid particles via a LJ potential (Fig.2, violet line)

$$U_{\text{LJ}}^{\text{graphene}}(r) \equiv 4\epsilon_g \left[\left(\frac{\sigma_g}{r}\right)^{24} + \left(\frac{\sigma_g}{r}\right)^6 \right] \quad (10)$$

with $\sigma_g = 3.26 \text{ \AA}$ and $\epsilon_g = 0.1 \text{ kcal/mol}$, which corresponds to the CHARMM27 force field [7]. We discuss an alternative potential for the graphene-fluids interactions in Appendix F. There, we also informed the values of the parameters we used to perform the simulations.

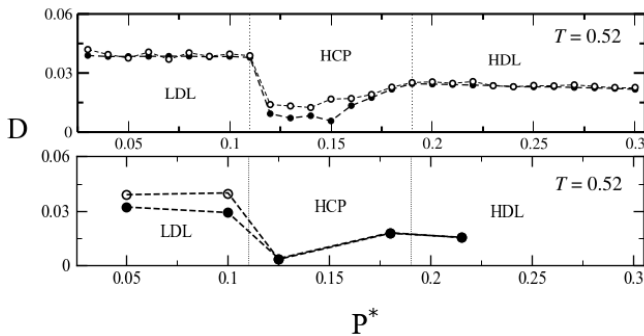


FIG. 3: Our setup and simulations with LAMMPS reproduce quantitatively the bulk diffusion coefficient D for water (filled symbols) and methanol center of mass (open symbols) of a 90%-10% CSW-methanol mixture at temperatures $T^* = 0.52$ over a range of pressures $0.050 \leq P^* \leq 0.125$. At low pressure the mixture is in a low-density-liquid (LDL) phase, at intermediate pressure in a hexagonal closed packed (HCP) crystal phase, and at high pressure in a high-density liquid (HDL) phase. The two phase transitions are marked by a change in D for each component. The agreement between the original simulation data from Ref. [10] (top) and our results (bottom) is good overall. We observe minor differences, possibly due to differences in the statistics and the pressurization process. Complete replication of the original results would imply a higher computational cost and is beyond the scope of the present work.

Similarly to before, we now have to add a few more relations of adimensional parameters:

$$\begin{aligned} \delta^* &\equiv \frac{\delta}{a}, \\ z^* &\equiv \frac{z}{a}. \end{aligned}$$

D. Bulk simulations

To check our setup, we first reproduce the bulk results for the diffusion constant of the 90% CSW- 10% methanol mixture as a function of pressure [10]. In the article, the methanol molecules are simulated using a dumbbell model to then study the diffusive dynamics of the fluid (CSW liquid-methanol dimer mixture) in the bulk, modifying the conditions of temperature and pressure. Thus, comparing our results against the ones presented in the original work will provide good foundations upon which to build the rest of the study.

Following Ref. [10], we set the total number of molecules in our system to $N = 1000$. This implies that for the 90%-10% mixture, we have 900 CSW particles and 100 dumbbells (100 methyl pseudoatoms and 100 hydroxyl pseudoatoms). We simulate the temperature $T^* = 0.52$ and five values of pressure, $P^* =$

0.050, 0.100, 0.125, 0.180, 0.125 over which one can observe two liquid-crystal phase transitions as a function of P [10]. We recover the original data with a good quantitative agreement (Fig. 3). However, the accuracy is not as high as it could be, mainly because of two factors: the first one is the fluctuation of the pressure. Fixing the pressure in a Molecular Dynamics simulation implies having a strong variation around the mean value, especially with smaller systems such as this one (1000 particles). The second one is the lack of statistics. Performing numerous times the same simulation for the same pressure would lead to the true value for the diffusion coefficient. This, however, would have implied a much larger time dedication. The simulation details for this section are reported in Appendix E.

Increasing P^* we observe that D for both mixture components drops at the pressure where, according to [10], the system undergoes a first-order phase transition from a low-density-liquid (LDL) phase to a hexagonal closed packed (HCP) crystal phase. By further increasing P^* , the crystal melts into a high-density liquid (HDL) phase [10]. This reentrant behavior is a consequence of the two length-scales of the CSW potential for the hydrogen-bonding groups and is typical of water-like liquids that gain entropy under pressurization. The smoothness of the change in D across the remelting suggests that the HCP-HDL phase transition has a different nature with respect to the LDL-HCP [10]. The investigation of this point goes beyond the scope of the present work.

E. Graphene slit-pore confinement

Next, we simulate the mixture nanoconfined in the graphene slit pore. We consider $N = 25,000$ molecules at constant temperature $T^* = 0.2$, constant V , and three mixture compositions: 100% CSW, 90%-10% CSW-methanol, and 75%-25% CSW-methanol. The first case allows us to compare with the results of CSW in slit-pore confinement in Ref. [7], while the other two with the bulk cases in Ref. [10].

Also, a mixture with 10% methanol can be considered as polluted water. Then, studying the evolution of the system could provide a few first ideas on how possible could be to obtain filtered water using this method. The more extreme case of a 25% mixture could be used to look into the industrial applications of the methodology we are studying.

For the pure CSW case, we fix the density $\rho_{\text{CSW}}^* = 0.201$. Apart from the excluded volume occupied by the graphene atoms,

$$\rho_{\text{bulk}}^* \approx \frac{25,000}{L_x L_y L_z} a^3.$$

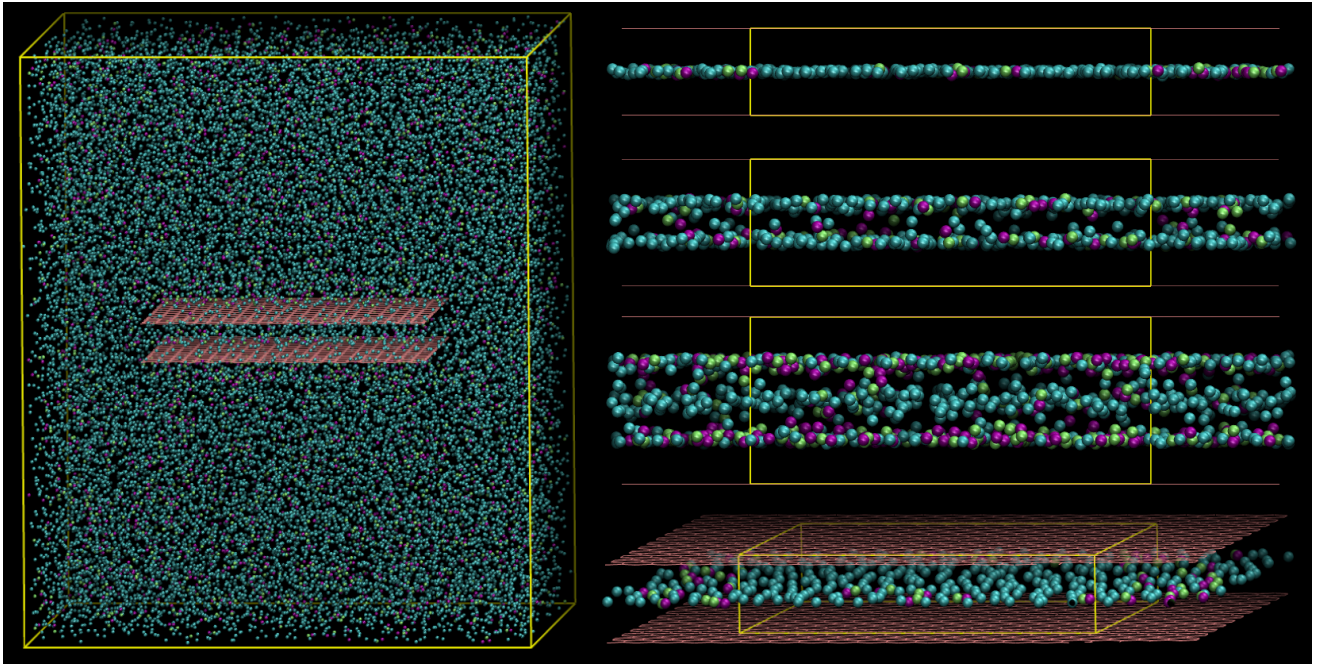


FIG. 4: Snapshots of the simulation with a 90%-10% CSW-methanol mixture, with CSW particles in blue, methyl pseudoatoms in purple, hydroxyl groups in green, graphene atoms in pink. (Left) Simulation box (in yellow) with the graphene slit-pore in its center and the mixture equilibrated at $T^* = 0.2$. (Right, from top to bottom) Side view of a mixture monolayer in the slit pore with $\delta^* = 3.67\text{\AA}$, a bilayer for the slit pore with $\delta^* = 5.37\text{\AA}$, a three-layer for $\delta^* = 7.06\text{\AA}$, a different view of the monolayer to emphasize the subvolume V^s (in yellow) used to compute the observables of the mixture under confinement. The panels are generated with the VMD visualization software.

Following Ref. [7], we fix $L_x = L_y = 84\text{\AA}$ and $L_z = 98\text{\AA}$. This numbers, once adimensionally converted, take the values:

$$\begin{aligned} L_x^* &= \frac{L_x}{a} = 47.458, \\ L_y^* &= \frac{L_y}{a} = 47.458, \\ L_z^* &= \frac{L_z}{a} = 55.367. \end{aligned}$$

We set the initial configuration by intertwining two hexagonal lattices (maximum packing) of water-like molecules and methanol dimers. The center of the simulation box is the same as the origin of coordinates, which means that our simulation box is located inside $-L_{xy}^*/2 < x, y < L_{xy}^*/2$ in the XY plane and $-L_z^*/2 < z < L_z^*/2$ in the remaining one.

We simulate the system in the NVT ensemble for 10^5 MD steps to properly mix the two liquids and use the following 10^5 MD steps to collect data every 100 MD steps, recording trajectories with 1000 positions and velocities for each particle.

It was necessary to record data every hundred steps because a file holding the totality of the readings (all the 10^5 MD steps) would be huge in terms of computational memory.

To minimize edge effects of the walls, we calculate each quantity for the confined mixture within a reduced region of the slit-pore, i.e., a central subvolume $V^s = L_x^s L_y^s \delta a^{-3}$, where δ is the separation between the sheets and $L_x^s = L_y^s = 30\text{\AA}$ (Fig. 4, yellow box).

The conversion to adimensional units, and the ones we will be using further on, are:

$$\begin{aligned} V^{s*} &= L_x^{s*} L_y^{s*} \delta^*, \\ L_x^{s*} &= L_x^s a^{-1} = 16.950, \\ L_y^{s*} &= L_y^s a^{-1} = 16.950. \end{aligned}$$

We compute the confined fluid density at distance z^* , perpendicular to the graphene sheets, from the center of the subvolume V^{s*} . We divide δ into 200 bins of size dz^* and calculate

$$\rho^*(z^*) \equiv \frac{\# \text{ molecules in } dz^*}{V^{s*}}. \quad (11)$$

Next, we compute the mean square displacement (MSD)

$$\begin{aligned} \Delta^2(t) &\equiv \langle (\vec{r}_i(t+t_0) - \vec{r}_i(t_0))^2 \rangle_\alpha = \\ &= N_\alpha^{-1} \sum_{i=1}^{N_\alpha} (\vec{r}_i(t+t_0) - \vec{r}_i(t_0))^2 \end{aligned} \quad (12)$$

where $\langle \rangle_{\alpha}$ is the thermal average calculated over the center of mass of the molecules α , with $\alpha = \text{CSW}$ or methanol, and over all the possible starting time t_0 . The diffusion coefficient will also be converted into adimensional units, using the relation:

$$\Delta^{2*} = \frac{\Delta^2}{a^2}$$

Given the planar geometry of the slit pore, we considered only the displacement parallel to the two sheets, considering negligible the diffusion along the orthogonal direction z^* . This observation is exact for a monolayer and it is reasonable for the bilayer and three-layer cases, given their sharpness, as discussed when we present the results for the density profiles.

As the methanol is formed by two particles, the MSD (and the density too) was computed using the Center of Mass (CM) of the dimer, with the expression:

$$r_{CM} = \frac{m_{\text{methyl}} r_{\text{methyl}} + m_{\text{OH}} r_{\text{OH}}}{m_{\text{methyl}} + m_{\text{OH}}} \quad (13)$$

We calculate the parallel diffusion coefficient as the large-time (diffusive regime) limit of the MSD slope

$$D_{\parallel} \equiv \lim_{t \rightarrow \infty} \frac{\Delta^2(t)}{4t} \quad (14)$$

where the 4 accounts for the two dimensions of the planar diffusion. The adimensional conversion of this magnitude follows this relation:

$$D_{\parallel}^* = D_{\parallel} \frac{t^*}{a^2}$$

Because we are interested in calculating D_{\parallel}^* within the confined subvolume V^{s*} , we check every 100 steps which particles are still within V^{s*} and use only them for our calculation. Then we fit linearly the MSD and extract D_{\parallel}^* from the resulting slope (Fig. 5).

III. RESULTS AND DISCUSSION

A. Density profile

The density profiles for the CSW liquid and the methanol confined in the slit pore recover the layering observed for pure CSW [7] and find it for each component in the different mixtures (Fig. 6). Specifically, as for pure CSW, for both components we observe a monolayer for a graphene separation $\delta = 6.5\text{\AA}$, two layers for $\delta = 9.5\text{\AA}$ and three layers for $\delta = 12.5\text{\AA}$. As we are using adimensional magnitudes, the conversion of the slit-pore width values are: $\delta^* = 3.67, 5.37, 7.06$. The monolayer is sharp around $z^* = 0$, as supported by eye inspection

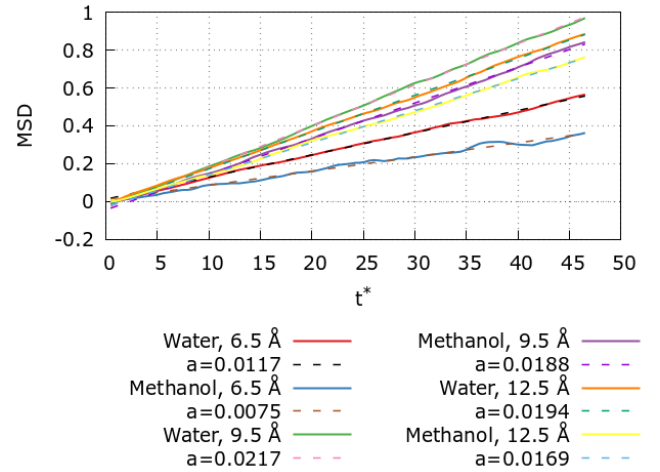


FIG. 5: Example of the linear fits (dashed lines) of the MSD for the confined CSW water-like particles and the methanol dumbbells within a graphene slit-pore with $\delta^* = 3.67$ (red and blue lines, respectively), $\delta^* = 5.37$ (green and purple lines), $\delta^* = 7.06$ (pink and yellow lines). The values of a and b in the legend are the linear and constant fitting parameters, respectively, of the calculated data, with $a = 4D_{\parallel}^*$.

(Fig.4, top right) and the values of the standard deviation in Table I in Appendix G.

By increasing δ^* , we observe that the central peak of the monolayer splits into two symmetric and more diffuse peaks (Fig.4, second top right) and, finally, into three symmetric peaks (Fig.4, third top right). For the CSW water-like model, the three peaks at $\delta^* = 7.06$ are similar in size with a slight predominance of the central layer. For the methanol, instead, the central peak is strongly depleted, while the two outer layers increase in population. The increase of methanol in the mixture, from 10% to 25%, emphasizes this effect.

The different distribution of water-like molecules and methanol among the three layers is a consequence of the preferential interaction of the methanol dumbbells with the graphene atoms, with twice as many interaction points as the CSW. It adequately mimics the amphiphilic property of methanol. Indeed, the apolar CH_3 group is expected to have a preferential interaction with the hydrophobic graphene, leaving more space for the hydrophilic water-like fluid in the central layer. Therefore, we expect that for a water-methanol mixture in a slit pore with $\delta^* \leq 7.06$ the methanol will populate the outer layers preferentially near the graphene walls, and the water would occupy the central part of the pore. This *segregation* effect suggests a possible qualitative difference in diffusion between the two components of the mixture.

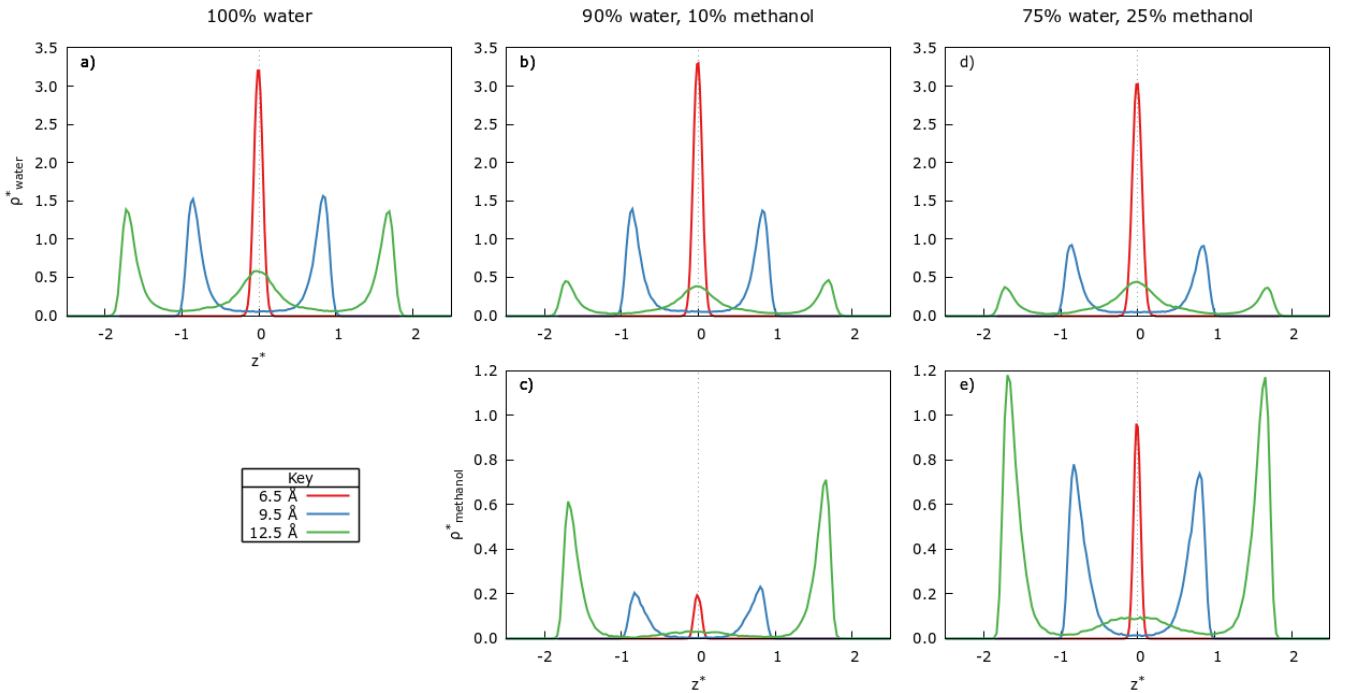


FIG. 6: Density profiles for the CSW liquid (top panels a, b, d) and the methanol (bottom panels c, e) for the three mixtures confined within a graphene slit-pore with $\delta^* = 3.67$ (red line), $\delta^* = 5.37$ (blue line), $\delta^* = 7.06$ (green line). (a) 100% CSW liquid, (b) and (c) 90%-10% CSW-methanol mixture, (d) and (e) 75%-25% CSW-methanol mixture.

B. Confined diffusion coefficient

Our calculation of the diffusion coefficient D_{\parallel}^* inside the slit pore and parallel to the walls for the components of the mixture shows a non-monotonic behavior as a function of the pore width δ^* (Fig.7 and Fig.8). At $\delta^* = 3.67$, the mixture forms a monolayer (Fig. 6) and the diffusion is minimum. We understand this result as a consequence of the interaction with the graphene walls. Because the interaction sites for the methanol dumbbells are twice as much as those for the CSW particles, the slowing-down effect is stronger for methanol than for the water-like liquid. Hence, the CSW D_{\parallel}^* is larger than that for methanol at any concentration (Fig.7).

At $\delta^* = 5.37$, both components form two layers near the two graphene walls (Fig. 6). The water-like liquid and the methanol interact on one side with the mixture via the two length scales of the CSW potential. The extra volume offered by the soft interaction facilitates the thermal diffusion of both components. The effect is limited for the methanol because only one of its two pseudoatoms interacts via the CSW. Hence, the methanol D_{\parallel}^* is smaller than that of the water-like liquid. Increasing the methanol concentration in the mixture decreases the facilitating effect (Fig.7).

At $\delta^* = 7.06$, the methanol populates the hydrophobic walls, while the water-like liquid concentrates more in the

central layer within the pore (Fig. 6). The slowing-down effect of the walls, as in the $\delta^* = 3.67$ case, competes with the facilitating effect of the soft interaction, as in the $\delta^* = 5.37$ case, determining a diffusion behavior that is intermediate between the two discussed so far. We find that the increase in methanol concentration affects the two components differently (Fig.7).

As a general rule of thumb, the more methanol in the mixture, the slower the thermal diffusion of the water-like liquid (Fig.8). We understand this result as a consequence of a steric effect. The larger proper volume of the methanol molecules reduces the free volume available for the CSW diffusion. Hence, the CSW D_{\parallel}^* decreases.

IV. SUMMARY AND CONCLUSIONS

We ask whether confining a mixture of a water-like liquid and methanol in a graphene slit pore would separate the two components by thermal fluctuations. Water-methanol mixtures are relevant in several industrial applications, including methanol filtration for water purification or methanol extraction for energetic uses. Still, their separation via traditional methods (distillation) is inefficient and economically expensive. Therefore, exploring alternative approaches is technologically significant and challenging from a fundamental physics stand-

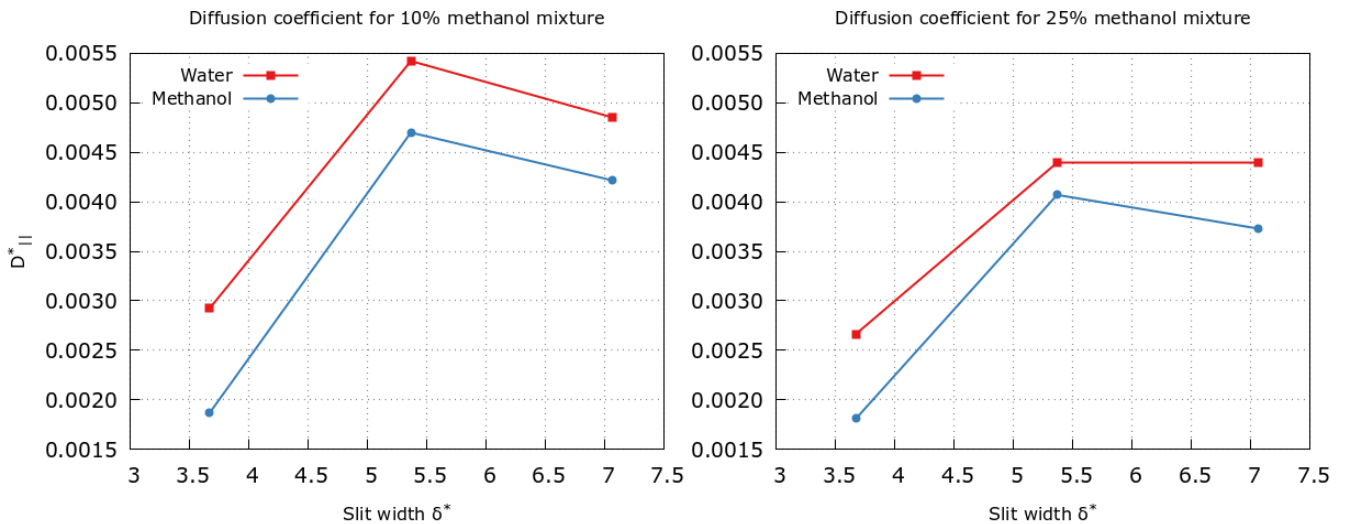


FIG. 7: The diffusion coefficient D_{\parallel}^* inside the slit pore and parallel to the walls for CSW water-like particles (red squares) and methanol dumbbells (blue circles) for the 90%-10% CSW-methanol mixture (left panel) and the 75%-25% CSW-methanol mixture (right panel) for the three values of the pore width δ^* considered in the present work. The diffusion coefficients are non monotonic and the value of the methanol D_{\parallel}^* is always smaller than that of the water-like liquid.

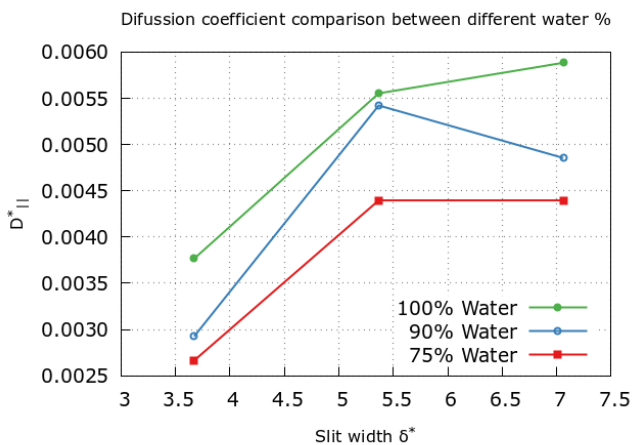


FIG. 8: The diffusion coefficient D_{\parallel}^* inside the slit pore and parallel to the walls for CSW water-like particles at different concentration in the CSW-methanol mixture, 100% (green full circles), 90% (open blue circles), and 75% (red squares) for the three values of the pore width δ^* considered in the present work. By increasing the methanol concentration in the mixture, the CSW D_{\parallel}^* decreases with an apparent change of the non monotonic behavior of D_{\parallel}^* vs. δ . Simulations for a larger number of values of δ^* , beyond the scope of this work, would be necessary to study the non-monotonicity of this relation.

point. Furthermore, it is timely given its relationship with two of the Sustainable Development Goals (SDGs) of the UN 2030 Agenda, the “Clean water and Sanitation” and the “Affordable and clean energy” goals.

With this aim, we simulate mixtures with different compositions in slit pores with different widths. We adopt coarse-grained models for water-like liquids and methanol. The CSW water-like liquid [9] and the dumbbell methanol model [11]. Both models have been tested in literature [12, 14] and they reproduce properties of the mixture considered here [10]. To test our model implementation, we reproduce the isothermal changes of the bulk diffusion of the mixture under pressurization. We find a good quantitative agreement with previous results showing a reentrant melting transition marked by drops in the bulk diffusion of the mixture [10].

Next, we confine mixtures with different methanol concentrations in a graphene slit pore. Previous results show that such confinement induces layering and a non-monotonic change of the diffusion coefficient for pure CSW water-like liquid when the pore width varies [7].

We reproduce the layering for pure CSW liquid and find an intriguing segregation effect for the mixture. The layering induces separation of the two components when at least three layers are in the pore. This is due to the larger number of interaction moieties of the methanol, compared to the water-like liquid, with the graphene atoms, and mimics the hydrophobic attraction between the two. The effect is more substantial when the mixture has more methanol. Hence, when enough layers are possible in the pore, the methanol accumulates near the graphene walls, while the water-like liquid populates more in the central part of the pore, away from the hydrophobic walls.

This result encourages us to explore the dynamic be-

havior of the confined mixture. As for pure CSW liquid, we observe a non-monotonic dependence, from the pore width, of the diffusion of the confined mixture components parallel to the graphene walls. In particular, the water-like liquid diffuses faster than the methanol, suggesting the possible separation of the two components by nanoconfinement.

Furthermore, the thermal diffusion decreases for both components when the methanol concentration rises. We understand that the CSW slows down due to a steric effect by increasing the methanol content in the mixture.

All these effects can be rationalized by considering the competition between two mechanisms. On the one hand, the methanol interacts more with the hydrophobic walls, slowing down the overall diffusion. On the other hand, the CSW soft interaction, mimicking the hydrogen bonds of the water-like liquid and the methanol hydroxyl group, facilitates the diffusion by providing free volume. The two mechanisms interplay giving rise to the non-monotonic dependence of the thermal diffusion coefficients from the pore width with different effects on each mixture component. Therefore, it is, in principle, possible to find an ideal pore width at which the separation by diffusion of the two mixture components is optimal.

A. Perspectives

There was a need to put some limits on the range of this work, which could be helpful or enlightening to work on in future research.

The first aspect to improve would be the reduced number of final data points provided. In the slit-pore simulations, only three out of the whole set of δ values were replicated. Adding more points could show a more detailed evolution of the behaviour of the system, completing this analysis and enabling a better comparison with the work developed by [7].

A second improvement could be the computation of the free energy and its components (the internal energy and the entropy) as the authors did in ref.[7]. Doing so would ease the comparison with the original results as well as provide information on which component drives each interaction.

It could also be considered to try mixtures with other alcohols like ethanol and 1-propanol. Minimalistic models for the mentioned molecules are studied in ref.[12],

together with the methanol one we used in this work. With this precedent, it would be fairly easy to compare results and obtain information.

Finally, the same simulations could be repeated at different temperatures and pressures. Obtaining information on the evolution of the measurable magnitudes (such as D_{\parallel} at different conditions could help into searching where the separation of the water-methanol mixture is optimal.

V. ACKNOWLEDGEMENTS

I thank Dr. Carles Calero and Dr. Fabio Leoni. They and my advisor answered my questions about the Molecular Dynamics simulations with LAMMPS and clarified my doubts about their published works.

Also, thanks to all family and friends for being there, support, and cheers.

Appendix A: Self-consistency problems on Nosé-Hoover thermostat

The Nosé-Hoover thermostat has a self-consistency problem that is solved by observing that, from

$$\begin{aligned} \mathbf{v}_i \left(t + \frac{\Delta t}{2} \right) &= \mathbf{v}_i \left(t - \frac{\Delta t}{2} \right) + \left[\frac{\mathbf{F}_i(t)}{m_i} - \xi(t) \mathbf{v}_i(t) \right] \Delta t \\ &= \mathbf{v}_i \left(t - \frac{\Delta t}{2} \right) + \frac{\mathbf{F}_i(t)}{m_i} \Delta t - \\ &\quad - \frac{\xi(t)}{2} \left[\mathbf{v}_i \left(t + \frac{\Delta t}{2} \right) + \mathbf{v}_i \left(t - \frac{\Delta t}{2} \right) \right] \end{aligned} \quad (\text{A1})$$

one gets

$$\begin{aligned} \mathbf{v}_i \left(t + \frac{\Delta t}{2} \right) &= \mathbf{v}_i \left(t - \frac{\Delta t}{2} \right) + \frac{\mathbf{F}_i(t)}{m_i} \Delta t - \\ &\quad - \frac{\xi(t)}{2} \mathbf{v}_i \left(t + \frac{\Delta t}{2} \right) - \frac{\xi(t)}{2} \mathbf{v}_i \left(t - \frac{\Delta t}{2} \right) \end{aligned} \quad (\text{A2})$$

$$\begin{aligned} \mathbf{v}_i \left(t + \frac{\Delta t}{2} \right) \left[1 + \frac{1}{2} \xi(t) \Delta t \right] &= \\ = \mathbf{v}_i \left(t - \frac{\Delta t}{2} \right) \left[1 - \frac{1}{2} \xi(t) \Delta t \right] + \frac{\mathbf{F}_i(t)}{m_i} \Delta t \end{aligned} \quad (\text{A3})$$

and, finally,

$$\mathbf{v}_i \left(t + \frac{\Delta t}{2} \right) = \left[1 + \frac{1}{2} \xi(t) \Delta t \right]^{-1} \left(\mathbf{v}_i \left(t - \frac{\Delta t}{2} \right) \left[1 - \frac{1}{2} \xi(t) \Delta t \right] + \frac{\mathbf{F}_i(t)}{m_i} \Delta t \right) \quad (\text{A4})$$

Appendix B: Details on the SHAKE algorithm

The SHAKE algorithm provides a way to impose distance constraints on groups of molecules. In this work, it is applied over a two-component molecule, but the number of components can be higher, at also a higher computational cost. The specifics of the method are the following:

1. Given the coordinates or a pair of particles i, j , some temporary positions are computed: $r_{pi}(t + \Delta t)$, $r_{pj}(t + \Delta t)$. This calculations are done without having in mind the constraints.
2. The second step is to compute the Lagrange multiplier associated to the constraint ($C(\mathbf{r}_i, \mathbf{r}_j) = 0$) at time $t + \Delta t$, thus obtaining:

$$\lambda = \frac{r_{pij}^2(t + \Delta t) - d^2}{4(m_i^{-1} + m_j^{-1})\Delta t^2 \mathbf{r}_{pij}(t + \Delta t) \cdot \mathbf{r}_{ij}(t)} \quad (\text{B1})$$

where d is the distance at which the particles are fixed. The computation to obtain the multiplier is developed in the next appendix section.

3. Then, the positions are corrected:

$$\begin{aligned} \mathbf{r}_i(t + \Delta t) &= \mathbf{r}_{pi}(t + \Delta t) + \frac{2\lambda\Delta t^2}{m_i} \mathbf{r}_{ij}(t) \\ \mathbf{r}_j(t + \Delta t) &= \mathbf{r}_{pj}(t + \Delta t) - \frac{2\lambda\Delta t^2}{m_j} \mathbf{r}_{ij}(t). \end{aligned} \quad (\text{B2})$$

4. Finally, after all particles have been swept, the algorithm checks for each i, j pair that the value $|r_{ij}^2 - d^2|$ is under a specified tolerance. If it is not, the algorithm restarts from the newest computed positions.

Appendix C: Obtention of the λ factor of the SHAKE procedure

To perform the SHAKE algorithm, it is necessary to modify the positions of the set atoms or molecules to fix them at a constant distance. To do so, it is required to compute a Lagrange multiplier that fulfills the imposed conditions on the system. Departing from equations B2, we combine them using the definition:

$$\mathbf{r}_{ij}(t) = \mathbf{r}_j(t) - \mathbf{r}_i(t) \quad (\text{C1})$$

to obtain:

$$\begin{aligned} \mathbf{r}_{ij}(t + \Delta t) &= \\ &= \mathbf{r}_{pij}(t + \Delta t) - 2\lambda\Delta t^2 \mathbf{r}_{12}(t) \left(\frac{1}{m_i} + \frac{1}{m_j} \right) \end{aligned} \quad (\text{C2})$$

From this point, we have to add the constraint condition:

$$C(\mathbf{r}_i, \mathbf{r}_j) = r_{ij}^2 - d^2 = 0$$

First, let's focus on the computation of r_{ij}^2 :

$$\begin{aligned} r_{ij}^2 &= \mathbf{r}_{ij} \cdot \mathbf{r}_{ij} = \\ &= r_{pij}^2(t + \Delta t) + 4\lambda^2 \Delta t^4 r_{ij}^2(t) \left(\frac{1}{m_i} + \frac{1}{m_j} \right)^2 - \\ &\quad - 4\lambda\Delta t^2 \mathbf{r}_{pij}(t + \Delta t) \cdot \mathbf{r}_{ij}(t) \left(\frac{1}{m_i} + \frac{1}{m_j} \right) \end{aligned} \quad (\text{C3})$$

where high orders such as $\mathcal{O}(\Delta t^4) \sim 0$, which makes the second term negligible. Replacing this expression into the constraint equation, we obtain:

$$C(\mathbf{r}_i, \mathbf{r}_j) = r_{ij}^2 - d^2 = r_{pij}^2(t + \Delta t) - 4\lambda\Delta t^2 \mathbf{r}_{pij}(t + \Delta t) \cdot \mathbf{r}_{ij}(t) \left(\frac{1}{m_i} + \frac{1}{m_j} \right) - d^2 = 0 \quad (\text{C4})$$

Now, isolating λ , we obtain:

$$\lambda = \frac{r_{pij}^2(t + \Delta t) - d^2}{4(m_i^{-1} + m_j^{-1})\Delta t^2 \mathbf{r}_{pij}(t + \Delta t) \cdot \mathbf{r}_{ij}(t)} \quad (\text{C5})$$

Appendix D: Computation of the relation between t and t^*

Recalling the expression that links the two magnitudes, we have:

$$t^* = \left(\frac{a^2 m}{U_A} \right)^{\frac{1}{2}} \quad (\text{D1})$$

Now, we must have in mind the proportions of the mixture we are dealing with, which is 10% methanol in 90%

water. Then:

$$m = 0.1 \times 32.04 + 0.9 \times 18.02 = 19.42 \frac{\text{g}}{\text{mol}} \quad (\text{D2})$$

which applied to the expression, yields:

$$\begin{aligned} t^* &= \left(\frac{a^2 m}{U_A} \right)^{\frac{1}{2}} = \\ &= \left(\frac{10^{-20} \text{\AA}^2 \times 19.42 \times 10^{-3} \text{kg/mol}}{4.184 \times 10^3 \text{J/mol}} \right)^{\frac{1}{2}} = \\ &= 2.15 \times 10^{-13} \text{ s} = 2.15 \times 10^2 \text{ fm} \end{aligned} \quad (\text{D3})$$

Appendix E: The NPT simulation protocol

1. First, we prepare the initial configuration of particles by intertwining two simple cubic lattices, the one on the outside composed of CSW liquid and the one on the inside with methanol dimers. Then, to thermalize the system, we simulate in the NVT ensemble using 5×10^6 timesteps with a time increment of $\delta t = 1$, in real units, as defined in Appendix D. In the original article, the time increment was set to $\delta t^* = 0.01$ in reduced units, so we take into account the difference between time scales to obtain the results in Fig.3. The computation of the relation between t and t^* is shown in Appendix D. We integrate the equations of motion using the Verlet algorithm, fixing the temperature via the Nosé-Hoover thermostat.
2. Then, to equilibrate the pressure of the system, we perform a second run of 1×10^6 timesteps in the NPT ensemble, with the same δt as before, adopting the Nosé-Hoover barostat and thermostat.
3. Finally, to calculate the mean square displacement (MSD) and the diffusion coefficient of the mixture components, we perform an NPT ensemble simulation along 1×10^7 timesteps with the δt unchanged.

In this first case, the MSD has been computed by the program LAMMPS itself, being able to trace its value along each timestep of the simulation.

Once we have obtained the necessary data, we avoid using the first values of the MSD as the diffusion coefficient is defined for large values of time.

Finally, we fit the diffusive regime of the MSD results with a linear function and its slope is divided by 6, thus obtaining the sought D value.

Appendix F: Alternative potential to the one used for the graphene sheets

The interaction of the graphene with the particles of the simulation could also be thought as an LJ potential with Lorentz-Berthelot mixing rules over the three existing potentials in the configuration. That would mean applying the mixing rules over:

$$\begin{aligned} LJ : \quad & \sigma_{LJ} = 1.77 \text{\AA}, \quad \epsilon_{LJ} = 0.02 \text{ kcal/mol} \\ LJ - LB : \quad & \sigma_{LB} = 1.77 \text{\AA}, \quad \epsilon_{LB} = 0.06 \text{ kcal/mol} \\ CSW : \quad & a = 1.77 \text{\AA}, \quad U_A = 0.2 \text{ kcal/mol} \end{aligned}$$

resulting in:

$$\begin{aligned} \sigma_{LB}^{graphene} &= \frac{\sigma_{LJ} + \sigma_{LB} + a}{3} = 1.77 \text{\AA} \\ \epsilon_{LB}^{graphene} &= \sqrt[3]{\epsilon_{LJ} \epsilon_{LB} U_A} = 0.06 \text{ kcal/mol} \end{aligned}$$

which differs significantly from the parameters of the potential used, specially in terms of σ . Here, we follow the Ref.[7] for the sake of comparison.

Appendix G: Data for the density profiles of the molecules inside the slit-pore.

-
- [1] R. R. Nair, H. A. Wu, P. N. Jayaram, I. V. Grigorieva, and A. K. Geim, "Unimpeded permeation of water through helium-leak-tight graphene-based membranes," *Science*, vol. 335, pp. 442–444, 01 2012.
- [2] J. Azamat, "Selective separation of methanol-water mixture using functionalized boron nitride nanosheet membrane: a computer simulation study," *Structural Chemistry*, vol. 30, no. 4, pp. 1451–1457, 2019.
- [3] P. Pršlja, E. Lomba, P. Gómez-Álvarez, T. Urbič, and E. G. Noya, "Adsorption of water, methanol, and their mixtures in slit graphite pores," *The Journal of Chemical Physics*, vol. 150, p. 024705, 2019/01/23 2019.
- [4] H. Mosaddeghi, S. Alavi, M. H. Kowsari, B. Najafi, S. Az'hari, and Y. Afshar, "Molecular dynamics simulations of nano-confined methanol and methanol-water mixtures between infinite graphite plates: Structure and dynamics," *The Journal of Chemical Physics*, vol. 150, p. 144510, 2020/05/27 2019.
- [5] P. G. Debenedetti, "Supercooled and glassy water," *Journal of Physics: Condensed Matter*, vol. 15, no. 45,

Slit (δ^*)	z range	% met.	Molec.	$\langle z^* \rho^* \rangle$	$\delta \langle z^* \rho^* \rangle$	$\sigma_{\langle z^* \rho^* \rangle}$
3.67	z_0	0	w	-0.0004	± 0.0005	0.0070
	z_0	10	w	-0.0004	± 0.0005	0.0072
	z_0	10	m	-1.8e-5	$\pm 2.3e-5$	0.0003
	z_0	25	w	-0.0004	± 0.0005	0.0073
	z_0	25	m	-8.4e-5	± 0.0001	0.0014
5.37	z_-	0	w	-0.0360	± 0.0093	0.0933
	z_+	0	w	0.0359	± 0.0093	0.0934
	z_-	10	w	-0.0324	± 0.0084	0.0842
	z_+	10	w	0.0314	± 0.0082	0.0815
	z_-	10	m	-0.0047	± 0.0012	0.0121
	z_+	10	m	0.0051	± 0.0013	0.0131
	z_-	25	w	-0.0223	± 0.0057	0.0572
	z_+	25	w	0.0219	± 0.0056	0.0555
	z_-	25	m	-0.0182	± 0.0046	0.0461
z_+	25	m	0.0171	± 0.0044	0.0435	
7.06	z_-	0	w	-0.0798	± 0.0222	0.1818
	z_0	0	w	-0.0008	± 0.0025	0.0207
	z_+	0	w	0.0759	± 0.0213	0.1753
	z_-	10	w	-0.0270	± 0.0074	0.0602
	z_0	10	w	-2.7e-6	± 0.0016	0.0127
	z_+	10	w	0.0264	± 0.0073	0.0599
	z_-	10	m	-0.0322	± 0.0095	0.0775
	z_0	10	m	9.1e-6	± 0.0003	0.0025
	z_+	10	m	0.0350	± 0.0105	0.0866
	z_-	25	w	-0.0222	± 0.0060	0.0489
	z_0	25	w	-0.0003	± 0.0018	0.0148
	z_+	25	w	0.0212	± 0.0058	0.0475
	z_-	25	m	-0.0643	± 0.0185	0.1518
	z_0	25	m	0.0004	± 0.0009	0.0072
	z_+	25	m	0.0613	± 0.0180	0.1475

TABLE I: Average density data for mixtures in slit pores with separation δ^* expressed in Angstroms (first column), at z position with z_- for the peaks at negative values of z , z_0 for those around $z = 0$ and z_+ for those at positive values of z (second column), with a fixed percentage of methanol in the mixture (third column), for the component "w" for the CSW water-like and "m" for methanol dimers (fourth column), the corresponding thermal average of the product of z and ρ , its related error and the standard deviation (column fifth, sixth and last, respectively).

pp. R1669–R1726, 2003.

- [6] C. Calero and G. Franzese, "Water under extreme confinement in graphene: Oscillatory dynamics, structure, and hydration pressure explained as a function of the confinement width," *Journal of Molecular Liquids*, vol. 317, p. 114027, 2020.
- [7] F. Leoni, C. Calero, and G. Franzese, "Nanoconfined fluids: Uniqueness of water compared to other liquids," *ACS Nano*, vol. 15, pp. 19864–19876, 12 2021.
- [8] P. Vilaseca and G. Franzese, "Softness dependence of the anomalies for the continuous shouldered well potential," *The Journal of Chemical Physics*, vol. 133, no. 8, p. 084507, 2010.
- [9] G. Franzese, "Differences between discontinuous and continuous soft-core attractive potentials: The appearance of density anomaly," *Journal of Molecular Liquids*, vol. 136, pp. 267–273, 12 2007.
- [10] M. S. Marques, V. F. Hernandez, E. Lomba, and J. Bordin, "Competing interactions near the liquid-liquid phase transition of core-softened water/methanol mixtures," *Journal of Molecular Liquids*, vol. 320, p. 114420, 2020.
- [11] M. Huš and T. Urbic, "Existence of a liquid-liquid phase transition in methanol," *Physical Review E*, vol. 90, pp. 062306–, 12 2014.
- [12] G. Munaò and T. Urbic, "Structure and thermodynamics of core-softened models for alcohols," *The Journal of Chemical Physics*, vol. 142, p. 214508, 2021/06/11 2015.
- [13]
- [14] A. B. de Oliveira, G. Franzese, P. A. Netz, and M. C. Barbosa, "Waterlike hierarchy of anomalies in a continuous spherical shouldered potential," *The Journal of Chemical Physics*, vol. 128, no. 6, p. 064901, 2008.